



QSP modeling of loncastuximab tesirine with T-cell-dependent bispecific antibodies guides dose-regimen strategy



Yuezhe Li¹, A. Katharina Wilkins¹, Jimena Davis¹, Timothy Knab¹, Marie Toukam², Joseph P. Boni² & Daniel C. Kirouac¹✉

Antibody-drug conjugates (ADCs) and T-cell-dependent bispecific antibodies (TDBs) show single-agent efficacy in relapsed/refractory (R/R) lymphomas. While coadministering therapeutics with orthogonal mechanisms of action may safely enhance efficacy, testing every potential combination regimen is infeasible in the clinic. An integrated quantitative systems pharmacology model of a CD19-targeted ADC and CD3/CD20-targeted TDBs was developed to predict combination regimen efficacy in R/R diffuse large B-cell lymphoma (DLBCL). Clinically validated models of the ADC loncastuximab tesirine and TDB mosunetuzumab were combined and extended to additional TDBs (glofitamab and epcoritamab). Virtual DLBCL populations were calibrated using monotherapy response data, and tumor volume dynamics simulated under alternate combination dosing regimens and patient scenarios. Additive antitumor effects were predicted from the fourth cycle onward, with combination efficacy insensitive to loncastuximab tesirine dose reductions or patient lymphopenias. Results of the LOTIS-7 study (NCT04970901) will soon be available to assess these predictions.

The treatment of cancer has been transformed over the last two decades through advances in antibody engineering technologies that specifically target cancer tissue, deliver therapeutic payloads, and modulate the cancer immunity cycle¹. These advances are exemplified in lymphoma, a diverse class of hematological cancers originating in the B-cell lineage². Rituximab, a CD20-targeted monoclonal antibody, was approved by the U.S. Food and Drug Administration (FDA) for the treatment of non-Hodgkin's lymphoma (NHL) in 1997. Arguably, the first targeted immunotherapy, receptor binding triggers both complement-mediated and antibody-dependent cellular cytotoxicity. In combination with chemotherapy (CHOP: cyclophosphamide, hydroxydaunorubicin, vincristine [Oncovin], and prednisone), R-CHOP is the first line of treatment for NHL. While R-CHOP cures 60% of patients, 15% are treatment refractory, and an additional 25% relapse within two years^{3,4}.

Although outcomes for patients with relapsed or refractory (R/R) disease remain poor, a plethora of options and treatment modalities are emerging with recent approvals. Three CD19-targeted chimeric antigen receptor T-cell (CAR-T) products have been FDA approved since 2017 with response rates in R/R NHL exceeding 70% and some durable responses exceeding a decade^{5,6}. However, autologous cell therapy product manufacturing brings a multitude of practical challenges⁷, which precludes the option for many patients⁸. T-cell-dependent bispecific antibodies (TDBs) and antibody drug conjugates (ADCs) are two alternative modalities with

proven efficacy in this patient population. Efficacy of both, however, remains capped by dose-limiting toxicities as well as mechanisms of intrinsic and acquired resistance⁹.

TDBs are a class of bispecific antibodies that simultaneously bind two targets: typically, the CD3 receptor on T cells and a tumor antigen. Trimer formation creates an immunological synapse and induces T-cell-mediated cytotoxicity without the requirement for clonal T-cell receptor (TCR) specificity, antigen presentation, or activation¹⁰. Four TDBs are FDA approved for the treatment of lymphoma: blinatumomab (2014), glofitamab (2023), mosunetuzumab (2022), and epcoritamab (2023), all of which engage CD3 and CD20. Response rates in R/R lymphoma patients typically exceed 50%, including patients who progressed following CD19-CAR-T treatment¹¹. Two general mechanisms underlie intrinsic and acquired resistance: loss of CD20 antigen expression and immunological suppression. TDBs are conditional agonists, dependent on the presence of cytotoxic effector T cells. T-cell activation and subsequent tumor response can thus be dampened by checkpoint expression (e.g., PD-L1), the presence of regulatory T cells (Tregs), myeloid-derived suppressor cells (MDSCs), immunosuppressive cytokines such as TGF-β and IL-10^{12,13}, as well as T-cell exhaustion¹⁴.

ADCs represent another means of targeting cancers by selectively delivering highly cytotoxic payloads to target-expressing tumor cells. Thirteen ADCs have been approved by the FDA to date, and more than 100 are in clinical testing for the treatment of various hematological and solid

¹Metrum Research Group, 68 Harrison Ave, Boston, MA, USA. ²ADC Therapeutics America, New Providence, NJ, USA. ✉e-mail: daniel.kirouac@metrumrg.com

tumors^{14,15}. Loncastuximab tesirine-lpyl, a CD19-targeted antibody linked to the potent warhead pyrrolobenzodiazepine (PBD), was approved for the treatment of R/R diffuse large B-cell lymphoma (DLBCL) in 2021. The overall response rate (ORR) in the phase-II registrational LOTIS-2 study (NCT03589469) was 48%, with a 27% complete response (CR) rate¹⁶. Resistance to ADCs as a class is mediated by intratumor heterogeneity. Selective pressures drive loss of target expression and metabolic changes, which reduce cellular sensitivity to payloads^{17,18}.

Combinations of modalities with different mechanisms of action (MoA) and non-overlapping dose-limiting toxicities (DLTs) are currently being investigated in multiple ongoing clinical trials¹⁹. This strategy aims to increase the breadth, depth, and duration of response without exacerbating toxicities. TDB/ADC combinations are an obvious choice in this regard. The main toxicity observed with TDB therapies is cytokine release syndrome (CRS), a consequence of hyper-activation of circulating T cells¹⁰. ADC DLTs are similar to standard chemotherapies: cytopenias, diarrhea and peripheral edema due to off-target payload exposure in the blood, gastrointestinal tract and lungs^{17,20}.

While dose optimization for combination regimens is a key component of FDA's Project Optimus²¹, the design space of clinical studies is limited by combinatorial complexity. Biological mechanism-based, quantitative systems pharmacology (QSP) models offer the opportunity to inform the design of such clinical trials via *in silico* testing of drug combination regimens²². By calibrating models to pharmacology and response data from individual agents, QSP models can potentially predict the effect of combinations and alternate dosing regimens prior to (or even in place of) clinical testing.

Herein, we apply this approach to inform the design of the LOTIS-7 clinical trial. It is a multi-arm study of A CD19-targeted ADC (loncastuximab tesirine) in combination with the TDBs mosunetuzumab and glofitamab (NCT04970901). An integrated QSP model of the two modalities was developed to predict combination regimen efficacy in R/R DLBCL. Specifically, model simulations were used to (1) assess whether independent MoAs of would result in additive, synergistic, or less-than-additive tumor responses; (2) select an optimal time for response assessment; (3) predict whether loncastuximab tesirine dose reduction would diminish efficacy; and (4) determine whether cytopenic patients would benefit from the combination regimen.

Given that clinically validated models of loncastuximab tesirine²³ and mosunetuzumab²⁴ were available in the public domain, these were simplified while maintaining core functionalities and combined. The integrated QSP model was then expanded to describe two other TDBs, glofitamab and epcoritamab, which are also approved for the treatment of DLBCL as monotherapies. Combination effects on tumor growth were then simulated under multiple dosing regimens and patient population scenarios. Results showed combination effects between loncastuximab tesirine and TDBs

appeared by the fourth treatment cycle, were insensitive to loncastuximab tesirine dose reductions and were maintained in lymphopenic patients. The accuracy of these predictions will soon be evaluated as results become available from the LOTIS-7 study.

Results

Simultaneous evaluation of CD19-ADC and CD20-TDB pharmacodynamics

As a qualitative predictive check, the integrated model was used to simulate monotherapy responses to the TDB monotherapies. Tumor size changes out to 12 weeks were simulated in a prototypic patient (responsive to either drug, based on parameterization from ref. 24) treated with mosunetuzumab, glofitamab, and epcoritamab monotherapies according to their approved dosing schemes; Fig. 1A). Tumor size reduction in this patient was comparable between glofitamab and epcoritamab, and both were greater than mosunetuzumab. The model-simulated tumor growth outcomes were consistent with relative response rates reported for the three agents, indicating that the differences in efficacy are explainable by PK and in vitro potency. Specifically, the ORRs to glofitamab and epcoritamab were approximately double that of mosunetuzumab, and CRs approximately tripled in R/R DLBCL²⁵. The differences in tumor responses also translated consistently to differences in progression-free survival and overall survival^{26,27}.

To assess the combination effects between loncastuximab tesirine and TDB regimens, tumor size changes were simulated in the same prototypical patient, now treated with mosunetuzumab monotherapy, loncastuximab tesirine monotherapy, and the combination dosing regimens from LOTIS-7 (Fig. 1B). The simulated tumor dynamics were notably different between treatment arms. Mosunetuzumab monotherapy was predicted to induce rapid tumor volume reduction over the first cycle, but this efficacy plateaus by D28. Loncastuximab tesirine, in contrast, maintained consistent anti-tumor activity over multiple treatment cycles, both alone and in combination. The combination regimen outperformed either monotherapy, but the comparative benefit on tumor reduction did not appear until cycle 4. That is, assessing the activity of these treatments depended on the time point at which tumor size measurements were evaluated.

Virtual population-based predictions of loncastuximab tesirine-lpyl and TDB combination regimen activity

To account for patient heterogeneity in treatment responses and benchmark simulations to available clinical data, a virtual population approach²² was applied to the model. Key physiological parameters and biomarkers were varied based on expected clinical ranges across the patient population (initial tumor volume, tumor proliferation rate, CD19/CD19 co-expression and ADC sensitivity; see Methods). The resulting virtual population ($n = 500$) accurately matched monotherapy response rates reported for

Fig. 1 | Tumor dynamic responses to TDB monotherapies and mosunetuzumab + loncastuximab tesirine combination therapy in a prototypic patient. **A** Comparison of tumor dynamics between TDB monotherapies. The TDB monotherapies were dosed following their corresponding labels. **B** Comparison of tumor dynamics between mosunetuzumab monotherapy, loncastuximab tesirine monotherapy, and mosunetuzumab + loncastuximab tesirine combination therapy, following the dosing scheme proposed in the LOTIS-7 study as described in the Methods, with the first 2 loncastuximab tesirine doses at 150 µg/kg. For both simulations, the tumor was composed of CD19⁺CD20⁺ B cells and had an initial volume of 49.5 mL, with a doubling time of 23 days²⁴. Lonca loncastuximab tesirine, TDB T-cell-dependent bispecific antibody.

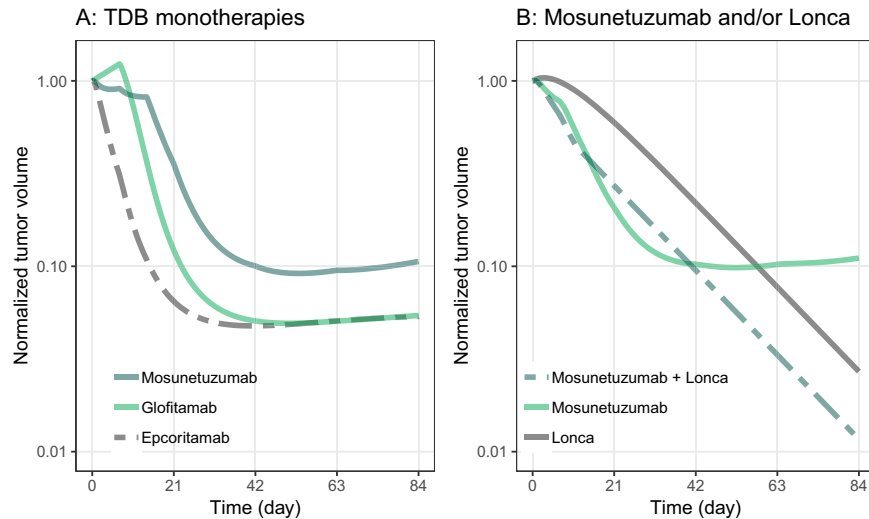


Table 1 | Observed versus simulated patient response rates to epcoritamab, mosunetuzumab, and loncastuximab-riensine monotherapy treatments

Epcoritamab		Mosunetuzumab		Loncastuximab tesirine	
Response	Sims	Obs	Sims	Obs	Sims
CR	43.68	43	18.63	20	28.05
PR	25.05	27	19.06	17	32.33
SD	3.21	4	7.92	7	16.7
PD	28.05	27	54.39	56	22.91

CR complete response, PR partial response, SD stable disease, PD progressive disease.

Response classifications are based on ref. 48.

Epcoritamab clinical data from $n = 157$ r/r NHL patients⁴⁶.

Mosunetuzumab clinical data from $n = 129$ aggressive-NHL patients⁴⁷.

Loncastuximab tesirine clinical data from $n = 145$ r/r DLBCL patients¹⁸.

Table 2 | Observed versus predicted patient response rates to glofitamab monotherapy treatment

Glofitamab (predictions)		
Response	Sims	Obs
CR	33.83	33
PR	13.28	15
SD	38.97	
PD	13.92	

CR complete response, PR partial response, SD stable disease, PD progressive disease.

The response classification is based on ref. 48.

Glofitamab clinical data from $n = 127$ aggressive-NHL patients²⁸.

epcoritamab, mosunetuzumab and loncastuximab tesirine treatments, as prescribed (Table 1) (response rates for the virtual cohort were reported in Supp. Table 5). Glofitamab response data²⁸ was not used in ‘prevalence weighting’ the virtual population. It was held out as a means of validating the model, and the response predictions were in very close agreement (Table 2).

Model simulations were then used to predict population-level tumor responses to loncastuximab tesirine-TDB combinations following 2 cycles of therapy (Day 42). For all three cases, greater efficacy was predicted for the combination than either agent alone (Fig. 2). Combination indices, calculated based on ORRs and a baseline assumption of Bliss Independence²⁹ indicated the effects were largely additive, rather than synergistic or antagonistic. This was not particularly surprising, given the independent mechanisms of action³⁰, but nonetheless promising. However, the combination index depends on evaluation time, as additive effects only appear beyond cycle 1 (Supp. Fig. 7).

To examine the mechanisms underlying therapeutic sensitivity and resistance, we computed rank correlations between model parameters vs. normalized tumor volume following treatment (Supp. Fig. 8). The results are in line with intuition and clinical observations. Tumor proliferation rate is non-specifically associated with treatment resistance³¹. Resistance to loncastuximab tesirine is associated with CD19-cell frequency, and parameters specifying payload-induced cell death³². Sensitivity to TDB treatment is associated with initial tumor size, which is somewhat non-intuitive. This results from the fact that TDB activity is contingent on the T:B-cell ratio³³, which is sub-optimal in very small tumors (Suppl Figs. 9 and 10). These results provide a degree of qualitative validation that the virtual population is representative of clinically meaningful biology.

Additional virtual population simulations were executed to explore the effect of potential loncastuximab tesirine dose reductions and number of treatment cycles on combination efficacy. In addition to the approved loncastuximab tesirine regimen (150 µg/kg Q3W for 2 cycles, followed by 75 µg/kg Q3W; 150/75), two reduced dosing regimens were simulated: 120 µg/kg Q3W for 2 cycles, followed by 75 µg/kg Q3W (120/75)

and 90 µg/kg Q3W (90). A breakdown of normalized tumor volume distribution by the end of each cycle (i.e., D21, D42, D63, D84, D105) revealed little difference in antitumor response between the three loncastuximab tesirine dosing regimens, while across all TDBs, the median tumor volume reduction was greater in combination with loncastuximab tesirine than without it (Fig. 3, Supp Fig. 11), as were the corresponding complete and partial response (PR) rates (Supp. Fig. 12). All combinations were predicted to reduce tumor volumes across the population over successive cycles, whilst TDB monotherapy effects plateau after cycle 1 or 2. That is, the loncastuximab tesirine dose may be reduced from the approved regimen with marginal effects on tumor volume reduction.

Variation in baseline patient T-cell and B-cell counts does not significantly affect the combination activity

Lymphoma patients are known to present as cytopenic with respect to both circulating B-cell and T-cell counts, due to effects of both disease and prior treatment history^{24,28}. A sensitivity analysis was thus carried out to investigate the impact of baseline T-cell and B-cell counts on treatment outcomes with either TDB monotherapy or loncastuximab tesirine combination therapy. As TDB efficacy is contingent on the formation of T-cell:drug-B-cell trimers, differences in the T-cell:B-cell ratio may be expected to alter efficacy in non-intuitive ways¹¹. Additionally, the PBD payload of loncastuximab tesirine has potential for non-specific cytopenias³⁴, which could manifest in reduced TDB potency. Epcoritamab was used as an example TDB, and baseline circulating T cells or B cells were reduced to 10% of the default, healthy population level.

A decrease in circulating T cells to 50% of baseline was predicted to minimally alter the epcoritamab + loncastuximab tesirine combination efficacy (Fig. 4A, right panel). However, a decrease in baseline circulating T-cell counts proportionally reduced the activity of epcoritamab monotherapy (Fig. 4A, left panel). Notably, the epcoritamab + loncastuximab tesirine combination was predicted to result in greater tumor volume reduction than epcoritamab monotherapy, regardless of baseline T-cell count by cycle 4. The results were qualitatively consistent for the TDBs glofitamab and mosunetuzumab and the respective loncastuximab tesirine combinations, though less pronounced (Supp. Fig. 13A).

A decrease in circulating B-cell counts by 20% of baseline had minimal effect on the epcoritamab + loncastuximab tesirine combination therapy effects (Fig. 4B, right panel). Decreases by up to 90% of baseline circulating B cells were predicted to minimally impact tumor response to epcoritamab monotherapy beyond cycle 2 (Fig. 4B, left panel). This was likely attributable to the depletion of healthy circulating B cells by CD20-engaging TDBs, thereby minimizing the effect over multiple cycles (Supp. Fig. 14). Again, the epcoritamab + loncastuximab tesirine combination was predicted to result in greater tumor volume reduction than epcoritamab monotherapy, regardless of baseline B-cell count by cycle 4. Similar predictions were observed for glofitamab and mosunetuzumab (Supp. Fig. 13B).

Fig. 2 | Virtual population responses to TDB and loncastuximab tesirine combinations following 2 cycles of therapy (Day 42). Combination indices (CI) were computed³⁷ to quantify the degree of non-additive effects resulting from the combinations (CI > 1 indicates synergy). (+/-) indicates presence/absence of loncastuximab tesirine. Dashed line: separation between nonresponders and responders. Tumor response classification based on ref. 50. TDB T-cell-dependent bispecific antibody, CI combination index.

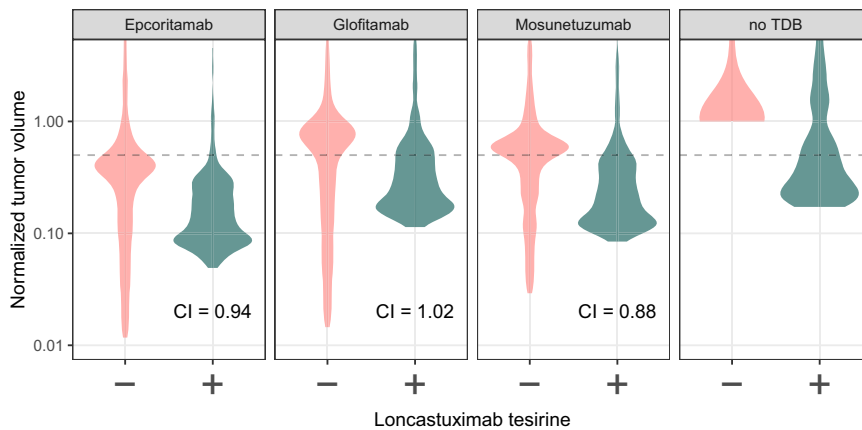
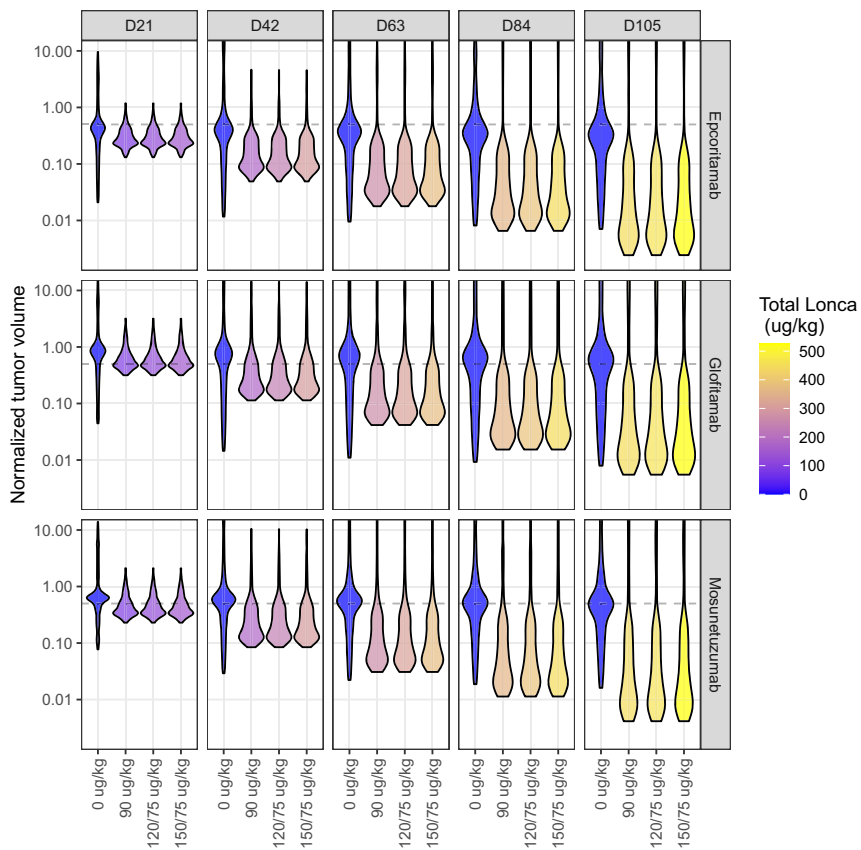


Fig. 3 | Virtual population responses to TDB and loncastuximab tesirine combination therapy by cycle and loncastuximab tesirine dosing regimen. Dashed line: separation between nonresponders and responders. Tumor response classification based on ref. 48. Lonca loncastuximab tesirine, TDB T-cell-dependent bispecific antibody.



Discussion

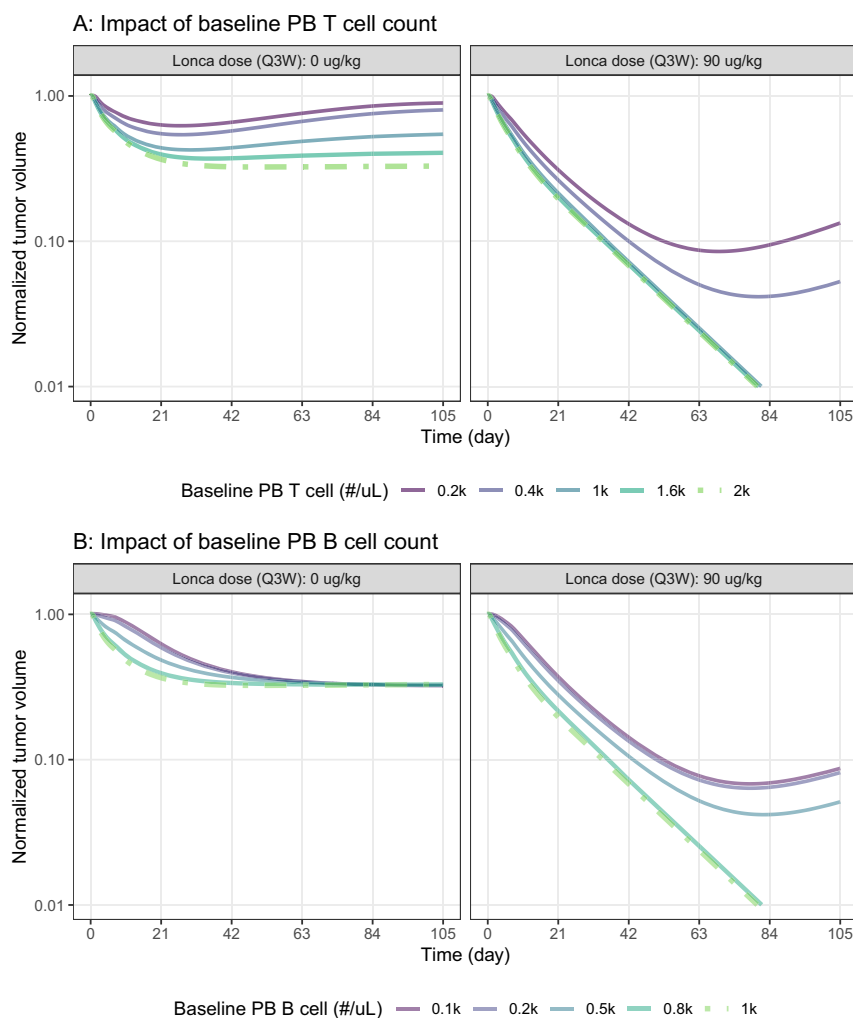
In this work, an integrated QSP model was developed to predict outcomes for R/R DLBCL patients treated with a combination regimen of alternate CD20-targeting TDBs and a CD19-targeted ADC, loncastuximab tesirine. Clinically validated³⁵ QSP models of loncastuximab tesirine and mosunetuzumab were combined and simplified to create an integrated platform model. To do so, the TDB model built to represent mosunetuzumab PKPD was extended to the alternate TDBs (i.e., glofitamab and epcoritamab) based on their in vitro potency and PK profiles, and the QSP model of loncastuximab tesirine was simplified to a 3-compartment PK model with semi-mechanistic description of cytotoxicity.

De novo model predictions of TDB monotherapies indicated similar tumor shrinkage between glofitamab and epcoritamab, with both outperforming mosunetuzumab. This projection was consistent with clinical observations and served as a qualitative validation. Model-predicted blood

T-cell changes during or after TDB treatment also corresponded well with clinical observations²⁸ (Supp. Fig. 3). These results served to increase confidence in the TDB component of the model.

A virtual population was created to account for patient heterogeneity and underlying physiological variance. Tumor responses simulated for this population precisely matched clinical observations reported for both the ADC, loncastuximab tesirine, and two TDBs, epcoritamab and mosunetuzumab. There are inevitable nuances and discrepancies when integrating clinical data from multiple studies. The finding that model simulations accurately predicted response rates to glofitamab, a treatment arm held out from prevalence weighting, lent confidence in the virtual population and subsequent predictions. Additionally, analyses of the virtual population recapitulated clinically established mechanisms of treatment sensitivity and resistance, a qualitative validation of the underlying biology.

Fig. 4 | Sensitivity of TDB (epcoritamab) and TDB + loncastuximab tesirine tumor responses to differences in initial circulating T-cell and B-cell counts. Default healthy baseline T-cell counts (A) were set at 2000 cells/uL, and default baseline B-cell counts (B) at 1000 cells/uL. The loncastuximab tesirine dose was set to be either 0 µg/kg or 90 µg/kg Q3W, with the epcoritamab dose following as described in the Methods. The tumor was assumed to have an initial volume of 7.5 mL with 80% CD19⁺CD20⁺ tumor B cells and 20% CD19 CD20⁺ cells. Lonca loncastuximab tesirine-lypil, PB peripheral blood, Q3W, every 3 weeks, TDB T-cell-dependent bispecific antibody.



The model predicted that TDB + loncastuximab tesirine combination therapy outperformed corresponding TDB or loncastuximab tesirine monotherapies by the end of cycle 4, with largely additive effects. This is perhaps not surprising. As the two therapeutics target unique cell surface receptors and employ distinct MoAs, we assumed linear additivity at the cellular level. However, there are non-linear system dynamics at play, which could potentially give rise to non-additive outcomes. The efficacy of TDBs is dependent on the ratio of T cells to B cells, hence the combination could have non-additive effects by altering this ratio. Indeed, this appears to be the case prior to cycle 4, where efficacy is less-than-additive.

In addition, reducing the first two loncastuximab tesirine doses from the approved regimen (150 µg/kg Q3W) to 90 µg/kg Q3W, a dose that showed efficacy in the LOTIS-1 study³⁶, had limited impact on the predicted tumor volume shrinkage. While simulations suggest loncastuximab tesirine monotherapy dose reductions from 150 to 90 µg/kg results in some loss of efficacy across the population, this is compensated for by the orthogonal activity of TDB treatment (Supp. Fig. 15). Antitumor efficacy of the combination was associated with the total number of treatment cycles administered, rather than the total dose of loncastuximab tesirine. These insights were crucial to the LOTIS-7 study design, providing a rationale for loncastuximab tesirine dose reductions that may reduce toxicity while maintaining comparable efficacy, and specifying a minimal time point for treatment evaluations.

Furthermore, the model predicted that TDB + loncastuximab tesirine combination activity is not particularly sensitive to initial T-cell or B-cell counts. Since lymphoma patients often present with cytopenias, this

indicates that the efficacy of combination therapies should be relatively robust in patients presenting with either disease- or therapy-mediated lymphopenias.

It is worth noting that the integrated model does not account for TDB or ADC-mediated toxicities. The original mosunetuzumab QSP model was calibrated to predict plasma IL-6 concentration²⁴, a biomarker of CRS. This model feature was not extended to glofitamab/epcoritamab due to the limited availability of data for model calibration. Additionally, while plasma IL-6 is often used as a CRS biomarker during dose escalation, it is an unreliable predictor of CRS risk^{37–39}. While the cellular activity of loncastuximab tesirine and any TDB was assumed as linearly additive due to the differing mechanisms, the impact of the combination on CRS and other toxicities is difficult to predict a priori.

Accuracy of the efficacy predictions will soon be evaluable as the LOTIS-7 data matures. While tumor response readouts can be used for model assessment and refinement, the toxicity readouts from this study will also be very informative. In particular, whether rates of CRS differ significantly from the TDB monotherapies. The model framework could then be used as a hypothesis exploration tool, assessing cellular mechanisms by which CD19-ADC treatment modulates (or does not) TDB-mediated CRS, which could then be used to inform future clinical studies.

Methods

Model structure

A system of ordinary differential equations (ODEs) was specified, consisting of 37 variables and 90 parameters. The model was built in a stepwise fashion

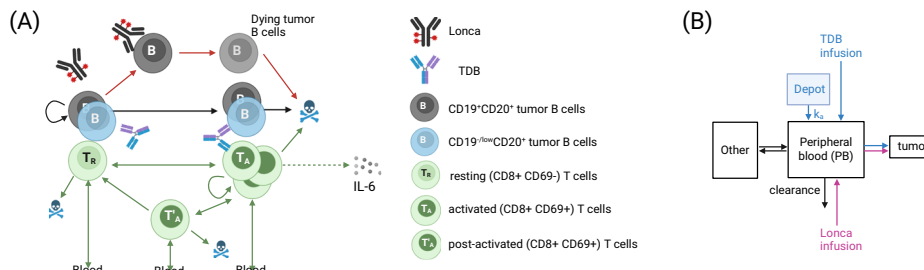


Fig. 5 | Schematic diagrams for the TDB + loncastuximab tesirine combination therapy model. **A** A compartmental PK diagram. The PK model includes three compartments: a central compartment (i.e., peripheral blood), a peripheral tissue compartment to account for drug distribution, and a deposit compartment to account for subcutaneous injection. **B** Tumor B-cell and T-cell dynamics in the presence of TDB and loncastuximab tesirine. T cells in the tumor cycle through resting state, activated state, and postactivated state (exhausted state), and may die at

any state. Only activated T cells proliferate and induce both healthy and cancerous B-cell death. All T cells could enter or leave the tumor from/the bloodstream. Loncastuximab tesirine could also induce the death of tumor B cells. Tumor cells killed by loncastuximab tesirine transition to a dying stage before being removed from the tumor. Lonca loncastuximab tesirine, PK pharmacokinetic, TDB T-cell-dependent bispecific antibody. Created in BioRender. Li, Y. (2025) <https://BioRender.com/nmbj785>.

by combining two published QSP models, one for the TDB mosunetuzumab²⁴ and the other for the ADC loncastuximab tesirine²³. The impact of TDB and ADC treatments on tumor cell viability were assumed to be additive, given they target distinct antigens (CD19, CD20) and have different mechanisms of action (DNA damage, T-cell-mediated cytotoxicity; Fig. 5A). Other potential crosstalks between the two drugs, such as the impact of free payload on T cells or inflammatory responses, were not incorporated due to the limited resolution on such molecular details. While at the cellular level we assume these mechanisms to be independent and additive, the non-linear system dynamics may result in non-additive effects on the primary clinical endpoint (tumor size assessment).

All parameters related to TDB pharmacokinetic/pharmacodynamic (PKPD) relationships were obtained from Hosseini et al.²⁴, unless specified in Supp. Tables 1 and 2. All loncastuximab tesirine-related PKPD parameters are listed in Supp Tables 2 and 4. Dynamics of TDB-dependent T-cell activation, B-cell killing, and tissue distribution were assumed to be conserved between peripheral blood, bone marrow, spleen and lymph nodes. Tissue distribution of both TDB and loncastuximab tesirine was described using a fixed set of partition coefficients, as reported²⁴.

Pharmacokinetics

A 3-compartment pharmacokinetic (PK) model was developed, comprising a central compartment (plasma), a peripheral tissue compartment, and a deposit compartment to account for subcutaneous injection of mosunetuzumab or epcoritamab (Fig. 5B). Bioavailability from the deposit compartment (depot) was assumed to be 0.7 for mosunetuzumab⁴⁰ and the absorption rate (k_a) to be 0.26 day⁻¹⁴¹. Compartment volumes, rates of distribution, and clearance were estimated based on published clinical PK profiles. For loncastuximab tesirine, clinical PK data were from the LOTIS-1 study (NCT02559017). For mosunetuzumab, median simulated data was from the patient label (obtained from www.accessdata.fda.gov), and glofitamab used PK data reported in Hutchings et al.²⁸ (Supp. Fig. 1A-C; parameters in Supp Table 2).

The PK model for epcoritamab was allometrically scaled from volumes and clearance parameters estimated from cynomolgus monkey PK⁴²] (Supp. Fig. 1D). The scaling was carried out based on body weight as $\theta_{\text{human}} = \theta_{\text{cyno}} \times (\frac{BW_{\text{human}}}{BW_{\text{cyno}}})^e$, with $e = 0.9$ for volume-related scaling and $e = 0.7$ for clearance/distribution-related scaling and with bioavailability adjusted to 0.95 to match the clinical PK profiles of epcoritamab as reported in the label⁴³. While the model structure and associated parameters differ from those used in the eventual BLA, simulations predict the reported clinical PK profiles well (Supp. Fig. 2).

Summary statistics of the simulated and reported PK were listed in Supp Table 3 (PK parameters in Supp. Table 2).

TDB pharmacodynamics

The TDB model was adapted from the mosunetuzumab QSP model developed by Hosseini et al.²⁴. In the tumor compartment, all tumor B cells were assumed to be CD20⁺. T cells were represented in three states: resting, activated, and exhausted. All T cells were assumed to be in the resting state prior to TDB dosing and then activated and exhausted following trimer formation with TDBs and B cells. The rate for TDB-dependent T-cell activation was described as

$$TDB_{act}^{Tumor} = VmT \times \left(\frac{\left(\frac{T_a^{Tumor}}{T_r^{Tumor} + T_a^{Tumor}} \right)^S}{\left(\frac{T_r^{Tumor}}{T_a^{Tumor}} \right)^S + (KmBT_{act}^{TDB})^S} \right) \times \frac{(TDB_{Tumor})^{TDB}_{act}}{(TDB_{Tumor})^{n_{act}^{TDB}} + (K_{act}^{TDB})^{n_{act}^{TDB}}} \quad (1)$$

where VmT represents the maximum rate for T-cell activation, $KmBT_{act}^{TDB}$ is the half maximal effective concentration (EC50) of B-cell to T-cell (B/T) ratio, K_{act}^{TDB} is the EC50 of TDB concentration, S and n_{act}^{TDB} are the Hill coefficients, T_r^{Tumor} and T_a^{Tumor} represent resting and activated T cells in the tumor, respectively, and B^{Tumor} represents tumor B cells. The rate of TDB-dependent B-cell death was described as

$$TDB_{kill}^{Tumor} = VmB \times \left(\frac{\left(\frac{T_a^{Tumor}}{B^{Tumor}} \right)^{n_{kill}^{TDB}}}{\left(\frac{T_r^{Tumor}}{B^{Tumor}} \right)^{n_{kill}^{TDB}} + (KmBT_{kill}^{TDB})^{n_{kill}^{TDB}}} \right) \times \frac{TDB_{Tumor}}{TDB_{Tumor} + K_{kill}^{TDB}} \quad (2)$$

where VmB represents the maximum rate for B-cell killing, $KmBT_{kill}^{TDB}$ is the EC50 of B/T ratio, K_{kill}^{TDB} is the EC50 of TDB concentration, n_{kill}^{TDB} is the Hill coefficient, T_a^{Tumor} represents activated T cells in the tumor, and B^{Tumor} represents tumor B cells.

The mosunetuzumab TDB model was adapted to describe the in vitro activity of glofitamab and epcoritamab. All EC50 values associated with T-cell activation and T-cell-induced B-cell killing (i.e., $KmBT_{act}^{TDB}$, K_{act}^{TDB} , K_{kill}^{TDB}) were optimized to minimize the mean squared error between predicted and observed in vitro cytotoxicity^{42,44} (Supp. Fig. 3; parameters in Supp Table 1).

Further in vivo validation was carried out by comparing the predicted and observed fold-change in circulating T-cell counts following glofitamab monotherapy²⁸ (Supp. Fig. 4). Observed data were collected from patients receiving 1000 mg obinutuzumab pre-treatment intravenously on day 0, 2.5 mg intravenous glofitamab on day 7, followed by 10 mg on day 14, then 16 mg or 30 mg every 3 weeks (Q3W) thereafter.

Loncastuximab tesirine pharmacodynamics

A QSP model of loncastuximab tesirine in patients with R/R DLBCL was previously developed and validated using data from the LOTIS-1 study (NCT02669017)²³. Simulations of this model were used to develop a functional equivalent with reduced complexity and amenable to integration with the TDB model PK and PD.

Loncastuximab tesirine-induced cytotoxicity was represented in a similar formulation as in the TDB model:

$$ADC_{kill}^{Tumor} = k_{kill}^{ADC} \times \frac{C_{ADC}^{n_{kill}}}{C_{Tumor}^{ADC} + EC50_{ADC}^{n_{kill}}} \quad (3)$$

where C_{Tumor}^{ADC} represents the loncastuximab tesirine concentration in the tumor, $EC50_{ADC}$ represents the EC50 concentration for loncastuximab tesirine-induced cell death, k_{kill}^{ADC} represents the maximum rate for loncastuximab tesirine-induced B-cell death, and n_{kill} represents the Hill coefficient. A cell distribution model⁴⁵ was implemented to describe the time lag between the induction of cell death and tumor clearance, as described in ref. 23. The dynamics of dying tumor B cells (B_{Tumor}^{dying}) was described as

$$\frac{d}{dt} B_{Tumor}^{dying} = ADC_{kill}^{Tumor} \times B_{Tumor} - k_{trans} \times B_{Tumor}^{dying} \quad (4)$$

where k_{trans} is the transition rate from cytotoxicity to tumor B-cell elimination, and B_{Tumor} represents healthy tumor B cells.

All parameters (k_{kill}^{ADC} , $EC50_{ADC}$, n_{kill} , k_{trans}) were optimized to minimize the L2 distance between predictions of tumor volume dynamics from the simplified model and those from the model with different CD19 expression levels per cell (Supp. Fig. 5; parameters listed in Supp Table 4). Specifically, the model aimed to capture two different populations of tumor B cells: CD19⁺CD20⁺ tumor B cells, defined as >10 CD19 epitopes per cell (Supp. Fig. 5, lower panels), and CD19^{-low}CD20⁺ tumor B cells, with 0–1 CD19 epitopes per cell (Supp. Fig. 5, upper panels). It should be noted that this threshold for CD19⁺ lies below the detection limit by routine experimental assays (e.g., via immunohistochemistry or flow cytometry), but was determined via simulated sensitivities to loncastuximab tesirine treatment²³.

Virtual population construction

Virtual populations were created by resampling (prevalence weighting) from a larger virtual cohort, such that monotherapy tumor responses matched reported clinical observations from three respective clinical trials, as described²². A virtual cohort of 20,000 subjects was generated by Latin Hypercube Sampling, five key parameters specifying initial tumor volumes, proliferation rates, CD19 expression heterogeneity, and ADC-mediated death rates between clinically feasible ranges. Initial tumor volumes were varied between 0.1 and 100 mL, and tumor proliferation rates between 0.00001 and 0.15 day⁻¹³³. Tumors were assumed to be a heterogeneous mix of CD19^{-low}CD20⁺ and CD19⁺CD20⁺ cells. The fraction of CD19^{-low}CD20⁺ was varied between 0 and 10%. Variance in ADC-mediated cytotoxicity was captured by varying k_{trans} for CD19⁺CD20⁺ cells between 0.01 and 0.05 day⁻¹, and k_{kill}^{ADC} for CD19^{-low}CD20⁺ cells between 0 and 0.07.

Prevalence weights were computed by matching simulated tumor responses to mosunetuzumab, epcoritamab, and loncastuximab tesirine monotherapy treatments from the approved regimens to their corresponding clinical observations^{16,46,47}. Relative tumor size changes at 6 or 12 weeks were categorized as CR, PR, stable disease (SD), or progressive disease (PD) based on thresholds of −78%, −50%, and +20%, respectively⁴⁸. Prevalence weights were then assigned via quadratic programming, and a Virtual Population of 500 patients was created by resampling with proportional frequencies so as to match single agent response frequencies, as described⁴⁹. Resampling statistics (Supp. Fig. 6) reveal the initial virtual cohort simulations covered the feasible clinical space well, but did not accurately predict response statistics de novo (Supp. Table

S5). Parametric characteristics of the resulting Virtual Population are reported in Supp Table S6.

Dosing schemes

Coadministration of loncastuximab tesirine and mosunetuzumab/glofitamab followed the protocol of the LOTIS-7 study (NCT05970901) for arm F/E, respectively, with each cycle spanning 21 days. Loncastuximab tesirine was dosed 120 µg/kg or 150 µg/kg Q3W for the first 2 cycles, followed by 75 µg/kg Q3W from cycle 3 and onward, or dosed 90 µg/kg continuously Q3W. Mosunetuzumab was dosed 5 mg subcutaneously on cycle 1 day 1 (C1D1), followed by 45 mg on cycle 1 day 8 (C1D8) and cycle 1 day 15 (C1D15), and then 45 mg Q3W from cycle 2 up to cycle 8.

Glofitamab was dosed according to clinical protocol²⁸, 2.5 mg intravenously on C1D8, 10 mg on C1D15, then 30 mg Q3W on D1 from cycles 2–12, with each cycle consisting of 21 days. The effect of obinutuzumab ‘debulking’ pre-treatment (1000 mg on C1D1) was simulated by depleting CD20⁺ B cells in blood, spleen, and bone marrow²⁸.

Coadministration of loncastuximab tesirine and epcoritamab followed the protocol proposed by Dr. Lorenzo Falchi of Memorial Sloan Kettering Cancer Center, with each cycle lasting 21 days. Epcoritamab was dosed intravenously at 0.16 mg, 0.8 mg, 48 mg on C1D1, C1D8, C1D15, respectively; then 48 mg on D1, D8, D15 between cycles 2 and 3; and then 48 mg Q3W onward. Loncastuximab tesirine was dosed the same as in combination therapy with mosunetuzumab or glofitamab.

It should be noted that the dosing schemes for mosunetuzumab and epcoritamab were different from their corresponding labels to more adequately mitigate toxicities, as based on the recent consensus of an international panel of academic and community-based practitioners⁵⁰. In the mosunetuzumab label, each dosing cycle consisted of 21 days, with 1 mg administered intravenously on C1D1, 2 mg on C1D8, 60 mg on C1D15, 60 mg on C2D1, and 30 mg Q3W from C3 onward. The dosing scheme for the epcoritamab label was based on 28 days per cycle. Epcoritamab is dosed subcutaneously 0.16 mg, 0.8 mg, 48 mg and 48 mg on C1D1, C1D8, C1D15, C1D22, respectively; then 48 mg QW on cycle 2 and 3; followed by 48 mg Q2W from cycle 4 onward.

Combination index

CI were calculated to assess combination synergy/antagonism relative to Bliss independence²⁹ based on response classification⁴⁸ at the end of each cycle. CI were calculated by dividing the simulated overall response rates (ORR = CR + PR) to combination treatments by the ORR predicted by independent activities:

$$ORR_{AB} = ORR_A + ORR_B \times (1 - ORR_A)$$

Software

All simulations were performed in Julia (v 1.7.2) using the Differential Equations package (v 7.10.0). Parameter optimizations were performed using the Nelder-Mead method implemented in the Optim package (v 5.15.2) or the Subplex algorithm implemented in the NLopt package (v 0.6.5). Prevalence weighting and sampling for the virtual population from the virtual cohort were computed in Julia (v 1.10) with packages Ipopt (v 1.6.6) and StatsBase (v 0.34.3). Visualizations were created using the Plots package (v 1.39.0) in Julia or the ggplot2 package (v 3.3.6) in R (v 4.1.2).

Data availability

Data Availability: all data was extracted or digitized from publications or FDA-documents. Mathematical model of loncastuximab tesirine: <https://pubmed.ncbi.nlm.nih.gov/38406517/> Mathematical model of mosunetuzumab: <https://pubmed.ncbi.nlm.nih.gov/32859946/> loncastuximab tesirine pharmacokinetics from LOTS-2 clinical study: <https://pubmed.ncbi.nlm.nih.gov/33989558/> StudyID NCT03589469: https://clinicaltrials.gov/study/NCT03589469?_a=29 Mosunetuzumab clinical pharmacokinetics, digitized from drug label: www.accessdata.fda.gov/drugsatfda_docs/label/2022/761263s000lbl.pdf Glofitamab clinical pharmacokinetics: <https://pubmed.ncbi.nlm.nih.gov/33739857/> Epcoritamab cyno-

pharmacokinetics: <https://pubmed.ncbi.nlm.nih.gov/31981978/> Epcoritamab clinical pharmacokinetics, from the BLA: www.accessdata.fda.gov/drugsatfda_docs/nda/2023/761324Orig1s000MultidisciplineR.pdf Mosunetuzumab and glofitamab in vitro potency: <https://pubmed.ncbi.nlm.nih.gov/29716920/> Epcoritamab in vitro potency: <https://pubmed.ncbi.nlm.nih.gov/31981978/> Glofitamab clinical T cell pharmacodynamics: <https://pubmed.ncbi.nlm.nih.gov/33739857/> Loncastuximab tesirine tumor response data: <https://pubmed.ncbi.nlm.nih.gov/37646659/> Epcoritamab tumor response data from: <https://pubmed.ncbi.nlm.nih.gov/36548927/> Mosunetuzumab tumor response data: <https://pubmed.ncbi.nlm.nih.gov/38547425/> Glofitamab tumor response data: <https://pubmed.ncbi.nlm.nih.gov/33739857/>.

Received: 4 February 2025; Accepted: 26 May 2025;

Published online: 11 June 2025

References

1. Scott, E. C. et al. Trends in the approval of cancer therapies by the FDA in the twenty-first century. *Nat. Rev. Drug Discov.* **22**, 625–640 (2023).
2. Tang, L., Huang, Z., Mei, H. & Hu, Y. Immunotherapy in hematologic malignancies: achievements, challenges and future prospects. *Signal Transduct. Target. Ther.* **8**, 306 (2023).
3. Dotan, E., Aggarwal, C. & Smith, M. R. Impact of rituximab (Rituxan) on the treatment of B-cell non-Hodgkin's lymphoma. *P T* **35**, 148–157 (2010).
4. Meng, F., Zhong, D., Zhang, L., Shao, Y. & Ma, Q. Efficacy and safety of rituximab combined with chemotherapy in the treatment of diffuse large B-cell lymphoma: a meta-analysis. *Int. J. Clin. Exp. Med.* **8**, 17515–17522 (2015).
5. Song, F. et al. Safety and efficacy of autologous and allogeneic humanized CD19-targeted CAR-T cell therapy for patients with relapsed/refractory B-ALL. *J. Immunother. Cancer* **11**, e005701 (2023).
6. Cappell, K. M. & Kochenderfer, J. N. Long-term outcomes following CAR T cell therapy: what we know so far. *Nat. Rev. Clin. Oncol.* **20**, 359–371 (2023).
7. Kirouac, D. C., Zmurchok, C. & Morris, D. Making drugs from T cells: The quantitative pharmacology of engineered T cell therapeutics. *npj syst. biol. appl.* **10**, 31 (2024).
8. Geethakumari, P. R., Ramasamy, D. P., Dholaria, B., Berdeja, J. & Kansagra, A. Balancing Quality, Cost, and Access During Delivery of Newer Cellular and Immunotherapy Treatments. *Curr Hematol Malignancy Rep* **16**, 345–356 (2021).
9. Dabkowska, A., Domka, K. & Firczuk, M. Advancements in cancer immunotherapies targeting CD20: from pioneering monoclonal antibodies to chimeric antigen receptor-modified T cells. *Front. Immunol.* **15**, 1363102 (2024).
10. Ball, K., Dovedi, S. J., Vajjah, P. & Phipps, A. Strategies for clinical dose optimization of T cell-engaging therapies in oncology. *MAbs* **15**, 2181016 (2023).
11. Falchi, L., Vardhana, S. A. & Salles, G. A. Bispecific antibodies for the treatment of B-cell lymphoma: promises, unknowns, and opportunities. *Blood* **141**, 467–480 (2023).
12. Mittal, S. K., Cho, K.-J., Ishido, S. & Roche, P. A. Interleukin 10 (IL-10)-mediated Immunosuppression: march-I induction regulates antigen presentation by macrophages but not dendritic cells. *J. Biol. Chem.* **290**, 27158–27167 (2015).
13. Yoshimura, A. & Muto, G. TGF-β function in immune suppression. *Curr. Top. Microbiol. Immunol.* **350**, 127–147 (2011).
14. Friedrich, M. J. et al. The pre-existing T cell landscape determines the response to bispecific T cell engagers in multiple myeloma patients. *Cancer Cell* **41**, 711–725.e6 (2023).
15. Tsuchikama, K., Anami, Y., Ha, S. Y. Y. & Yamazaki, C. M. Exploring the next generation of antibody-drug conjugates. *Nat. Rev. Clin. Oncol.* **21**, 203–223 (2024).
16. Caimi, P. F. et al. Loncastuximab tesirine in relapsed/refractory diffuse large B-cell lymphoma: long-term efficacy and safety from the phase II LOTIS-2 study. *Haematologica* **109**, 1184–1193 (2024).
17. Nguyen, T. D., Bordeau, B. M. & Balthasar, J. P. Mechanisms of ADC toxicity and strategies to increase ADC tolerability. *Cancers* **15**, 713 (2023).
18. Olivier, K. J., Jr & Hurvitz, S. A. *Antibody-drug conjugates: fundamentals, drug development, and clinical outcomes to target cancer*. (John Wiley & Sons, 2016).
19. Zhu, W. M. & Middleton, M. R. Combination therapies for the optimisation of Bispecific T-cell Engagers in cancer treatment. *Immunother. Adv.* **3**, Itad013 (2023).
20. Tolcher, A. W. Antibody drug conjugates: lessons from 20 years of clinical experience. *Ann. Oncol.* **27**, 2168–2172 (2016).
21. Gao, W. et al. Realizing the promise of Project Optimus: Challenges and emerging opportunities for dose optimization in oncology drug development. *CPT Pharmacomet. Syst. Pharm.* **13**, 691–709 (2024).
22. Gadkar, K., Kirouac, D. C., Mager, D. E., van der Graaf, P. H. & Ramanujan, S. A Six-Stage Workflow for Robust Application of Systems Pharmacology. *CPT Pharmacomet. Syst. Pharm.* **5**, 235–249 (2016).
23. Caimi, P. F. et al. In relapsed or refractory diffuse large B-cell lymphoma, CD19 expression by immunohistochemistry alone is not a predictor of response to loncastuximab tesirine. *EJHaem* **5**, 76–83 (2024).
24. Hosseini, I. et al. Mitigating the risk of cytokine release syndrome in a Phase I trial of CD20/CD3 bispecific antibody mosunetuzumab in NHL: impact of translational system modeling. *npj Syst. Biol. Appl.* **6**, 1–11 (2020).
25. Liu, X., Zhao, J., Guo, X. & Song, Y. CD20 × CD3 bispecific antibodies for lymphoma therapy: latest updates from ASCO 2023 annual meeting. *J. Hematol. Oncol.* **16**, 90 (2023).
26. Salvaris, R., Ong, J. & Gregory, G. P. Bispecific antibodies: a review of development, clinical efficacy and toxicity in B-cell lymphomas. *J. Pers. Med.* **11**, 355 (2021).
27. Dada, R. Redefining precision management of r/r large B-cell lymphoma: novel antibodies take on CART and BMT in the quest for future treatment strategies. *Cells* **12**, 1858 (2023).
28. Hutchings, M. et al. Glofitamab, a novel, bivalent CD20-targeting t-cell-engaging bispecific antibody, induces durable complete remissions in relapsed or refractory B-cell lymphoma: a phase I trial. *J. Clin. Oncol.* **39**, 1959–1970 (2021).
29. Fouquier, J. & Guedj, M. Analysis of drug combinations: current methodological landscape. *Pharmacol. Res. Perspect.* **3**, e00149 (2015).
30. Hwangbo, H., Patterson, S. C., Dai, A., Plana, D. & Palmer, A. C. Additivity predicts the efficacy of most approved combination therapies for advanced cancer. *Nat. Cancer* **4**, 1693–1704 (2023).
31. Anbari, S. et al. Identifying biomarkers for treatment of uveal melanoma by T cell engager using a QSP model. *npj Syst. Biol. Appl.* **10**, 1–12 (2024).
32. Ascione, L. et al. Unlocking the potential: biomarkers of response to antibody-drug conjugates. *Am. Soc. Clin. Oncol. Educ. Book* **44**, e431766 (2024).
33. Susilo, M. E. et al. Systems-based digital twins to help characterize clinical dose-response and propose predictive biomarkers in a Phase I study of bispecific antibody, mosunetuzumab, in NHL. *Clin. Transl. Sci.* **16**, 1134–1148 (2023).
34. Saber, H., Simpson, N., Ricks, T. K. & Leighton, J. K. An FDA oncology analysis of toxicities associated with PBD-containing antibody-drug conjugates. *Regul. Toxicol. Pharmacol.* **107**, 104429 (2019).
35. Kirouac, D. C. How Do We 'Validate' a QSP Model?. *CPT Pharmacomet. Syst. Pharm.* **7**, 547–548 (2018).
36. Hamadani, M. et al. Final results of a phase 1 study of loncastuximab tesirine in relapsed/refractory B-cell non-Hodgkin lymphoma. *Blood* **137**, 2634–2645 (2021).

37. Morris, E. C., Neelapu, S. S., Giavridis, T. & Sadelain, M. Cytokine release syndrome and associated neurotoxicity in cancer immunotherapy. *Nat. Rev. Immunol.* **22**, 85–96 (2022).
38. Radtke, K. K. et al. Clinical pharmacology of cytokine release syndrome with T-cell-engaging bispecific antibodies: current insights and drug development strategies. *Clin. Cancer Res.* **31**, 245–257 (2025).
39. Wei, Z. et al. Prediction of severe CRS and determination of biomarkers in B cell-acute lymphoblastic leukemia treated with CAR-T cells. *Front. Immunol.* **14**, 1273507 (2023).
40. Gill, K. L., Gardner, I., Li, L. & Jamei, M. A bottom-up whole-body physiologically based pharmacokinetic model to mechanistically predict tissue distribution and the rate of subcutaneous absorption of therapeutic proteins. *AAPS J.* **18**, 156–170 (2016).
41. Kapitanov, G. I. et al. A mechanistic site-of-action model: a tool for informing right target, right compound, and right dose for therapeutic antagonistic antibody programs. *Front. Bioinform.* **1**, 731340 (2021).
42. Engelberts, P. J. et al. DuoBody-CD3xCD20 induces potent T-cell-mediated killing of malignant B cells in preclinical models and provides opportunities for subcutaneous dosing. *EBioMedicine* **52**, 102625 (2020).
43. Epkinly (epcoritamab) dosing, indications, interactions, adverse effects, and more. <https://reference.medscape.com/drug/epkinly-epcoritamab-4000342> (2024).
44. Bacac, M. et al. CD20-TCB with obinutuzumab pretreatment as next-generation treatment of hematologic malignancies. *Clin. Cancer Res.* **24**, 4785–4797 (2018).
45. Yang, J., Mager, D. E. & Straubinger, R. M. Comparison of two pharmacodynamic transduction models for the analysis of tumor therapeutic responses in model systems. *AAPS J* **12**, 1–10 (2010).
46. Thieblemont, C. et al. Epcoritamab, a novel, subcutaneous CD3xCD20 bispecific T-cell-engaging antibody, in relapsed or refractory large b-cell lymphoma: dose expansion in a phase I/II trial. *J. Clin. Oncol.* **41**, 2238–2247 (2023).
47. Budde, L. E. et al. Single-Agent Mosunetuzumab Shows Durable Complete Responses in Patients With Relapsed or Refractory B-Cell Lymphomas: Phase I Dose-Escalation Study. *J. Clin. Oncol.* **40**, 481–491 (2022).
48. Cheson, B. D. et al. Revised response criteria for malignant lymphoma. *J. Clin. Oncol.* **25**, 579–586 (2007).
49. Kirouac, D. C. et al. Clinical responses to ERK inhibition in -mutant colorectal cancer predicted using a computational model. *NPJ Syst. Biol. Appl.* **3**, 25 (2017).
50. Crombie, J. L. et al. Consensus recommendations on the management of toxicity associated with CD3xCD20 bispecific antibody therapy. *Blood* **143**, 1565–1575 (2024).

Acknowledgements

We would like to thank Sara Miller for editorial assistance. This work was supported by ADC Therapeutics SA and partially funded by Sobi.

Author contributions

Wrote manuscript: Y.L., A.K.W., D.K., J.P.B. Designed research: Y.L., A.K.W., D.K., J.P.B. Performed Research: Y.L., A.K.W., T.K., J.D., M.T. Analyzed data: M.T.

Competing interests

Y.L., A.K.W., J.D., T.K., and D.C.K. are employees of Metrum Research Group. M.T. is an employee and current equity holder at ADC Therapeutics. J.B. is an equity holder at ADC Therapeutics and was employed at ADC Therapeutics when the study was conducted.

Additional information

Supplementary information The online version contains supplementary material available at <https://doi.org/10.1038/s41540-025-00544-8>.

Correspondence and requests for materials should be addressed to Daniel C. Kirouac.

Reprints and permissions information is available at <http://www.nature.com/reprints>

Publisher's note Springer Nature remains neutral with regard to jurisdictional claims in published maps and institutional affiliations.

Open Access This article is licensed under a Creative Commons Attribution-NonCommercial-NoDerivatives 4.0 International License, which permits any non-commercial use, sharing, distribution and reproduction in any medium or format, as long as you give appropriate credit to the original author(s) and the source, provide a link to the Creative Commons licence, and indicate if you modified the licensed material. You do not have permission under this licence to share adapted material derived from this article or parts of it. The images or other third party material in this article are included in the article's Creative Commons licence, unless indicated otherwise in a credit line to the material. If material is not included in the article's Creative Commons licence and your intended use is not permitted by statutory regulation or exceeds the permitted use, you will need to obtain permission directly from the copyright holder. To view a copy of this licence, visit <http://creativecommons.org/licenses/by-nc-nd/4.0/>.

© The Author(s) 2025